

# New Vibrational Numbering and Potential Energy Curve for the $3^3\Pi_g$ Electronic State of the $\text{Li}_2$ Molecule

V. S. Ivanov,\* V. B. Sovkov,\* L. Li,† A. M. Lyyra,‡ G. Lazarov,‡ and J. Huennekens§

\*Russian Center for Laser Physics and Institute of Physics, St. Petersburg State University, 1 Ulyanovskaya Street, Petrodvorets, St. Petersburg, 198904 Russia; †Department of Modern Applied Physics, Tsinghua University, Beijing, 100084 China; ‡Department of Physics, Temple University, Philadelphia, Pennsylvania 19122; and §Department of Physics, Lehigh University, 16 Memorial Drive East, Bethlehem, Pennsylvania 18015

Received April 8, 1998; in revised form October 29, 1998

An experimental study of the  $3^3\Pi_g$  electronic state of  $^7\text{Li}_2$ , using the Perturbation-Facilitated Optical-Optical Double Resonance (PFOODR) technique, was recently reported [A. Yiannopoulou *et al.*, *J. Chem. Phys.* **103**, 5898, (1995)]. However, due to the very small number of known  $^7\text{Li}_2$   $A^1\Sigma_u^+ \sim b^3\Pi_u$  window levels, only 13 ro-vibrational levels (spanning a range of vibrational levels designated  $v_x - 1$  to  $v_x + 3$  in that reference) could be observed. Dunham coefficients, based on the assignment  $v_x = 7$ , were found to fit the observed term values and give a qualitative fit to the intensities of the first six lines of the  $3^3\Pi_g$  ( $v = v_x, N = 11$ )  $\rightarrow b^3\Pi_u$  emission spectrum. However, due to the limited number of levels used in the fit, both the absolute vibrational numbering and the  $3^3\Pi_g$  RKR potential curve obtained from the Dunham coefficients, must be considered to be uncertain. In the present work, we show that the previously reported  $3^3\Pi_g$  RKR curve is unable to reproduce the experimental intensity distribution in the  $^7\text{Li}_2$   $3^3\Pi_g$  ( $v_x = 7, N = 11$ )  $\rightarrow a^3\Sigma_u^+$  emission continuum. We report new experimental data for the  $^7\text{Li}_2$   $3^3\Pi_g$  ( $v_x + 1, N = 11$ )  $\rightarrow a^3\Sigma_u^+$  bound-free continuum and discrete  $3^3\Pi_g$  ( $v_x \pm 1, N = 11$ )  $\rightarrow b^3\Pi_u$  spectra obtained using the PFOODR experimental technique. We demonstrate that the correct vibrational numbering and an improved RKR potential curve can be obtained by analyzing the experimental term values in combination with all observed bound-free and discrete spectra. Finally, term values for four  $^6\text{Li}_2$   $3^3\Pi_g$  ro-vibrational levels were obtained using PFOODR spectroscopy. The measured isotope shifts confirm the absolute vibrational numbering obtained from the present analysis. © 1999 Academic Press

## 1. INTRODUCTION

Alkali diatomic molecules have been studied extensively over the last several decades because they are theoretically tractable and their electronic transitions can be pumped using visible and near IR tunable dye lasers.  $\text{Li}_2$ , in particular, has attracted considerable attention because, except for  $\text{H}_2$ , it is the simplest stable homonuclear molecule. Most experimental studies of the alkali molecules have concentrated on the spin-singlet electronic states due to the dipole selection rule on spin ( $\Delta S = 0$ ) and the fact that the ground state  $X^1\Sigma_g^+$  is a singlet. The development of Perturbation-Facilitated Optical-Optical Double Resonance (PFOODR) spectroscopy in 1983 (1) has opened the door to the study of the triplet electronic states of the alkali molecules. In this technique, advantage is taken of mutually perturbing pairs of levels such as  $A^1\Sigma_u^+$  ( $v_A, J$ )  $\sim b^3\Pi_u$  ( $v_b, J$ ). Nearly degenerate levels of these two states, which have the same  $J$ , are coupled by the spin-orbit interaction. The resulting mixed states have both singlet and triplet character. High-lying triplet states can then be accessed from these mixed singlet-triplet window levels in a double-resonance experiment.

Recently, Yiannopoulou *et al.* (2) reported PFOODR studies of the  $^7\text{Li}_2$   $2^3\Pi_g$  and  $3^3\Pi_g$  electronic states using the only known  $^7\text{Li}_2$   $A^1\Sigma_u^+ \sim b^3\Pi_u$  window levels ( $A^1\Sigma_u^+$  ( $v' = 13, J' = 4$ )  $\sim b^3\Pi_u$  ( $v' = 19, N' = 5$ ),  $A^1\Sigma_u^+$  ( $v' = 13, J' =$

$7$ )  $\sim b^3\Pi_u$  ( $v' = 19, N' = 7$ ), and  $A^1\Sigma_u^+$  ( $v' = 13, J' = 11$ )  $\sim b^3\Pi_u$  ( $v' = 19, N' = 10$ )). The  $2^3\Pi_g$  state was well characterized since transitions into a wide range of  $2^3\Pi_g$  vibrational levels ( $v = 0-41$ ) were observed. However, large Franck-Condon factors exist only for a limited number of transitions into levels of the  $3^3\Pi_g$  electronic state from the  $A^1\Sigma_u^+ \sim b^3\Pi_u$  window levels. Thus, only 13 ro-vibrational levels of the  $3^3\Pi_g$  state were observed (spanning a range of vibrational levels designated  $v_x - 1$  to  $v_x + 3$ ). The absolute vibrational numbering was difficult to determine and the  $3^3\Pi_g$  ( $v = v_x, N = 11$ ) rovibrational level with the term value  $35\,491.452\text{ cm}^{-1}$  was assigned to  $v_x = 7$  in Ref. (2), based on a counting of nodes in the bound-free  $3^3\Pi_g$  ( $v = v_x, N = 11$ )  $\rightarrow a^3\Sigma_u^+$  continuum, and a simulation of intensities for the first six lines of the bound-bound  $3^3\Pi_g$  ( $v = v_x, N = 11$ )  $\rightarrow b^3\Pi_u$  emission spectrum. However, this numbering was considered uncertain because the long wavelength end of the bound-free continuum is overlapped by the short wavelength end of the stronger  $3^3\Pi_g \rightarrow b^3\Pi_u$  bound-bound emission, while the long wavelength end of the latter is, in turn, strongly overlapped by  $A^1\Sigma_u^+ \rightarrow X^1\Sigma_g^+$  fluorescence lines (produced by both the pump and probe lasers individually). Moreover, the limited range of observed rotational and vibrational levels requires the fitting of a limited number of Dunham coefficients for the  $3^3\Pi_g$  state. The long extrapolation to the bottom of the

potential well is necessarily uncertain, and the RKR potential constructed from the Dunham coefficients reflects that same uncertainty. For this reason, calculated Franck–Condon factors for  $3^3\Pi_g \rightarrow b^3\Pi_u$  transitions must also be considered suspect.

In light of recent work by two of us (3–5) devoted to the development of new techniques for inverting experimental spectroscopic data to yield adiabatic potential curves of molecules, we set out to simulate the intensity distribution of the bound-free  $3^3\Pi_g$  ( $v = v_x, N = 11$ )  $\rightarrow a^3\Sigma_u^+$  continuum. Calculations based on the  $^7\text{Li}_2$   $3^3\Pi_g$  RKR potential reported in (2) (based on the assignment  $v_x = 7$ ) did not allow us to reproduce the experimental spectrum. We have, therefore, carried out additional measurements at Temple University to record the  $3^3\Pi_g$  ( $v = v_x + 1, N = 11$ )  $\rightarrow a^3\Sigma_u^+$  continuum and the short wavelength sections of the  $3^3\Pi_g$  ( $v = v_x \pm 1, N = 11$ )  $\rightarrow b^3\Pi_u$  discrete spectra, as well as more complete  $3^3\Pi_g$  ( $v = v_x, N = 11$ )  $\rightarrow b^3\Pi_u$  bound–bound emission scans. These have been combined with the previous  $3^3\Pi_g$  ( $v = v_x, N = 11$ )  $\rightarrow a^3\Sigma_u^+$  continuum spectrum and the term values reported in (2) in a global fit to determine the correct vibrational numbering and an improved RKR potential, which are presented below. We believe this technique, which makes use of bound–bound and bound-free emission spectra, in addition to measured term values, is useful for determining more accurate experimental potential curves in cases where only a limited number of levels can be observed.

As a final check of the vibrational numbering, we have carried out measurements of term values for four ro-vibrational levels of the  $^6\text{Li}_2$   $3^3\Pi_g$  state using the window level  $A^1\Sigma_u^+$  ( $v' = 9, J' = 20$ )  $\sim b^3\Pi_u$  ( $v' = 15, N' = 19$ ) (6) of that isotopomer. The isotope shift provides an absolute determination of the vibrational numbering and confirms the results of the global fit of the  $^7\text{Li}_2$  data. These  $^6\text{Li}_2$   $3^3\Pi_g$  term values have been combined with all available  $^7\text{Li}_2$  data in one last global fit to calculate a final or best RKR potential for the  $\text{Li}_2$   $3^3\Pi_g$  state.

## 2. RESULTS

As a first step, we carried out a direct simulation of the intensity distribution in the  $^7\text{Li}_2$   $3^3\Pi_g$  ( $v = v_x, N = 11$ )  $\rightarrow a^3\Sigma_u^+$  continuum, using computer programs implementing the Numerov–Cooley–Blatt method (7) with the initial  $v_x = 7$  vibrational numbering and the five spectroscopic constants  $T_e$ ,  $Y_{10}$ ,  $Y_{20}$ ,  $Y_{01}$ , and  $Y_{11}$  from (2) (see also Table 1). For the repulsive electronic state  $a^3\Sigma_u^+$ , we have taken the theoretical potential energy curve from (8). This potential function was used previously in computations of the  $^7\text{Li}_2$   $2^3\Pi_g$  ( $v = 17, N = 4$ )  $\rightarrow a^3\Sigma_u^+$  and  $^7\text{Li}_2$   $3^3\Sigma_g^+$  ( $v = 10, N = 10$ )  $\rightarrow a^3\Sigma_u^+$  transition continua (4) and was found to reproduce the experimental spectra with good accuracy. Note that the line intensities in the  $^7\text{Li}_2$   $3^3\Sigma_g^+$  ( $v = 10, N = 10$ )  $\rightarrow b^3\Pi_u$  transition were also simulated with good accuracy in (9), confirming the high quality of the  $b^3\Pi_u$  potential curve of Ref. (10). The

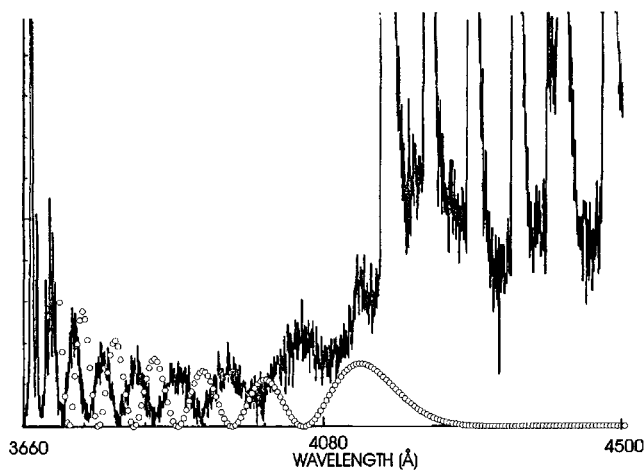
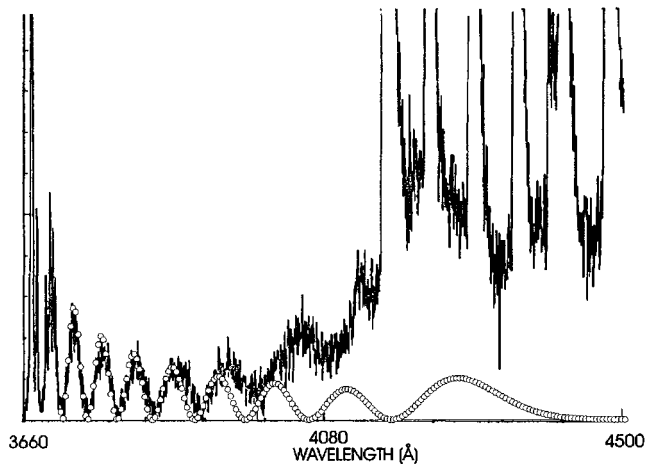


FIG. 1. Experimental  $^7\text{Li}_2$   $3^3\Pi_g$  ( $v = v_x, N = 11$ )  $\rightarrow a^3\Sigma_u^+$  bound-free continuum and corresponding initial simulation based upon the vibrational numbering  $v_x = 7$  and the  $3^3\Pi_g$  state RKR potential from (2).

Condon approximation,  $M(R) = \text{constant}$  (where  $M(R)$  is the transition dipole moment as a function of internuclear separation  $R$ ), was used in our initial calculations. The other details of the simulation were the same as in (4). The basic approach is as follows. First, the Schrödinger equation is solved numerically for the upper bound state potential to yield the nuclear radial wavefunction corresponding to the particular ro-vibrational level of interest. Next, the Schrödinger equation is again solved for the lower repulsive potential, to yield the free state wavefunction corresponding to the continuum level which lies below the upper bound state by the energy of the emitted photon ( $hc/\lambda$ ). If the transition dipole moment is assumed to be constant with  $R$ , then the emission intensity at  $\lambda$  is simply proportional to the square of the upper and lower state wavefunction overlap integral. The complete spectrum is obtained by calculating the emission intensity as a function of wavelength (i.e., calculating the upper and lower state wavefunction overlaps for various levels lying at different energies within the lower state continuum). The result of this first simulation is shown in Fig. 1. The computed and experimental spectra differ strongly.

The intensity distribution depends on the electronic state potentials and on the transition moment operator  $M(R)$ . The influence of  $M(R)$  on the node positions in the continuum is very weak (4, 11), so the node positions can be used as criteria for the quality of the potentials.

One of the possible origins of this inability of the simulation to reproduce the experimental continuum can be the wrong vibrational numbering of the observed terms. We have tried to simulate the continuum with other vibrational numberings,  $v_x = 8$  and  $v_x = 9$ . In the simulations, analogous to (2), the five spectroscopic constants  $T_e$ ,  $Y_{10}$ ,  $Y_{20}$ ,  $Y_{01}$ , and  $Y_{11}$  were fitted using the observed ro-vibrational term values from (2) (see also Table 4 of the present work), and the RKR potential energy curve was constructed for the  $3^3\Pi_g$  state using each assumed



**FIG. 2.** Experimental  ${}^7\text{Li}_2\ 3^3\Pi_g\ (v = v_x, N = 11) \rightarrow a^3\Sigma_u^+$  bound-free continuum and corresponding initial simulation based upon the vibrational numbering  $v_x = 9$ .

vibrational numbering. The closest match to the observed spectrum is the case  $v_x = 9$  (Fig. 2). On the other hand, the vibrational numberings  $v_x = 8$  and  $v_x = 9$  could not explain the line intensities in the  ${}^7\text{Li}_2\ 3^3\Pi_g\ (v_x, N = 11) \rightarrow b^3\Pi_u$  transition. These facts together show that no vibrational numbering is able to accurately account for all the experimental data through the approach described above.

Next, we tried to apply the WKB nodes method (5) to derive the bound state potential function from the continuum. This method gave the vibrational numbering  $v_x = 9$ , but its accuracy was too low to consider this result unambiguous, especially since part of the experimental continuum is difficult to observe because it is buried beneath the strong bound-bound  $3^3\Pi_g\ (v_x, N = 11) \rightarrow b^3\Pi_u$  spectrum.

The origin of the inconsistency between the simulations of the line intensities and the continuum can be found by analyzing all factors that can influence the observations. The node positions in the continuum can only be affected appreciably by potentials; namely, the bound  $3^3\Pi_g$  state potential in the case considered here. The line intensities can be affected by the following factors: (i) the potential function; (ii) a possible strong variation of the transition moment operator  $M(R)$ ; and (iii) nonadiabatic perturbations of the  $b^3\Pi_u$  levels. Strong nonadiabatic perturbations of the  $b^3\Pi_u$  levels can be excluded here based on the results of the line intensity simulation for the  ${}^7\text{Li}_2\ 3^3\Sigma_g^+\ (v = 10, N = 10) \rightarrow b^3\Pi_u$  transition in (9), a case where all available experimental data were in good agreement with each other. If strong variation of the  $M(R)$  function with  $R$  appreciably influenced the line intensities, then the agreement between the observed and simulated line intensities observed with the  $v_x = 7$  numbering would have to be considered accidental. It is highly unlikely that the same accidental coincidence would take place for transitions from other vibrational levels  $v \neq v_x$ . We have now checked this possibility by carrying out new experimental investigations.

Intensities for the first seven lines of the  ${}^7\text{Li}_2\ 3^3\Pi_g\ (v_x \pm 1, N = 11) \rightarrow b^3\Pi_u$  spectra have now been measured by the same experimental method as in (2). The new continuum,  ${}^7\text{Li}_2\ 3^3\Pi_g\ (v_x + 1, N = 11) \rightarrow a^3\Sigma_u^+$ , was also measured and used in the analysis. Simulations of the new spectra show that the situation remains the same; all line intensities are reproduced with rather good accuracy if  $v_x = 7$  is assumed, but this assumption does not allow us to reproduce the continua. Instead, the continua are reproduced rather well if  $v_x = 9$  is assumed, but this assumption is inconsistent with the experimental line spectra. The only conclusion that can be made is that the RKR potential function of the  $3^3\Pi_g$  state, constructed as described above, is at least somewhat in error for any vibrational numbering.

A schematic diagram of the  $\text{Li}_2$  potential energy curves which are relevant to the current discussion is given in Fig. 3. It can be seen from the figure that line intensities, arising from transitions into the lowest rovibrational levels of the  $b^3\Pi_u$  state, are determined primarily by the left (short-range) limb of the  $3^3\Pi_g$  state potential energy curve. These lines form the short wavelength end of the bound-bound  $3^3\Pi_g \rightarrow b^3\Pi_u$  band which is most accurately observed and analyzed in the experiment. On the other hand, the short wavelength end of the bound-free  $3^3\Pi_g \rightarrow a^3\Sigma_u^+$  continuum, which is most clearly observed in the experiment, is determined primarily by the right (long-range) limb of the  $3^3\Pi_g$  potential. Therefore, we can conclude that the true potential function should behave approximately like the one obtained by assuming  $v_x = 7$  at small internuclear separations, and like the one obtained using  $v_x = 9$  at large separations.

Although the Dunham representation for the ro-vibrational terms through a set of  $Y_{ij}$  constants is widely applied, it is also well known that this approach is not unique (12, 13). A truncated Dunham series is a good representation for term values located near the bottom of a potential well, or perhaps in another limited region of energies far from the dissociation

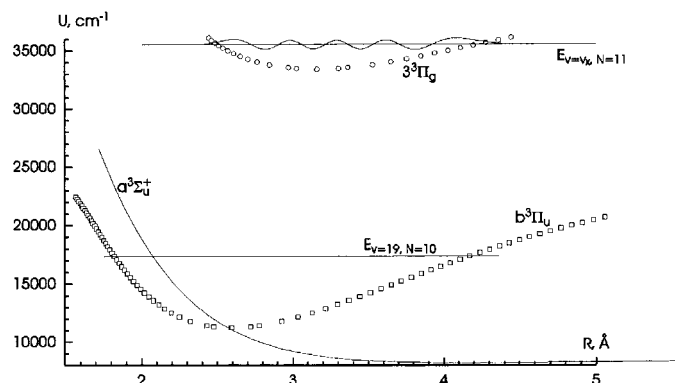


**FIG. 3.** Potential energy curves of the  $\text{Li}_2$  molecule (see text for details). Positions of the ro-vibrational levels  $b^3\Pi_u\ (v = 19, N = 10)$  (excitation window level),  $3^3\Pi_g\ (v = v_x, N = 11)$ , and the wavefunction of the latter state are shown.

TABLE 1  
Spectroscopic Constants of the  $\text{Li}_2$   $3^3\Pi_g$  State

	spectroscopic constants from [2] <sup>1</sup>	spectroscopic constants determined in this work using $^7\text{Li}_2$ data	final spectroscopic constants determined in this work using all data	theoretical spectroscopic constants <sup>2</sup>
$T_e$	33638.53136	33410.003	33406.385	33456.318
$Y_{10}$	253.3639233	248.8951	249.8826	246.2885
$Y_{20}$	-1.865760821	-1.01066	-1.07737	-1.35082
$Y_{30}$		-3.0550(-2)	-3.0508(-2)	-1.9488(-2)
$Y_{01}$	0.5183202293	0.481777	0.49142	0.47653
$Y_{11}$	-1.034563494(-2)	-2.5259(-3)	-6.3226(-3)	-5.2066(-3)
$Y_{21}$		-2.7520(-4)	5.7447(-5)	-3.7072(-5)
$Y_{02}$			-7.6021(-6)	-7.1358(-6)
$R_e$	3.044873	3.158	3.127	3.176

Note. All constants are in units of  $\text{cm}^{-1}$  with the exception of  $R_e$  which is in  $\text{\AA}$ .

<sup>1</sup> The original Dunham coefficients reported in (2) were based on 11 of the 13 term values reported in Table III of Ref. (2) (the  $v = v_x + 3$ ,  $N = 9$ , and  $v = v_x + 1$ ,  $N = 4$  terms were excluded). The Dunham coefficients listed here are based on 12 of the 13 term values (only  $v = v_x + 1$ ,  $N = 4$  was excluded). All calculations presented in the current work and described as based on the constants of (2) are actually based on the very slightly revised set of constants given here.

<sup>2</sup> The theoretical spectroscopic constants in the Table 1 differ from the ones reported in (2). Unfortunately, the latter were incorrect; this can be seen from the inconsistency of the  $R_e$  and  $Y_{01}$  values reported in (2) ( $R_e = 3.175 \text{ \AA}$  corresponds to  $Y_{01} = 0.477 \text{ cm}^{-1}$ , rather than the value  $Y_{01} = 0.538 \text{ cm}^{-1}$  reported in (2)). The new theoretical spectroscopic constants given here were estimated by smoothing the points of the theoretical potential function given in (2) with the Pade-SVD technique, calculating a set of rovibrational levels, and fitting spectroscopic constants to them.

limit. The wider the range of vibrational quantum levels  $v$  to be described, the more spectroscopic constants must be used. The limited number of rovibrational levels that could be observed in (2), using the three known  $^7\text{Li}_2$  window levels, precluded the fitting of more than the five spectroscopic constants  $T_e$ ,  $Y_{10}$ ,  $Y_{20}$ ,  $Y_{01}$ , and  $Y_{11}$  to the observed term values. However, it is clear that while this limited set of constants may reproduce the observed level positions in the range of  $v = (v_x - 1) - (v_x + 3)$ , it is not sufficient to accurately represent levels down to the bottom of the potential well. Consequently, the  $3^3\Pi_g$  RKR potential function obtained as described above is unable to reproduce the bound-bound and bound-free spectra, which depend in detail on the lower portions of the potential curve. To successfully simulate these spectra, a more complete set of spectroscopic constants is needed.

The following fitting procedure has been used to find a more complete set of spectroscopic constants.

1. Initial values for additional fitting constants  $Y_{30}$  and  $Y_{21}$  were chosen.

2. The other spectroscopic constants  $T_e$ ,  $Y_{10}$ ,  $Y_{20}$ ,  $Y_{01}$ , and  $Y_{11}$  were fitted from the observed ro-vibrational level positions

reported in (2) (see Table 4 of the present work) with these fixed values of  $Y_{30}$  and  $Y_{21}$ .

3. The RKR potential function was constructed from the full set of spectroscopic constants.

4. The experimentally observed continua and line intensities were simulated using this RKR potential function in the same manner as described above.

5. Corrections to the initial  $Y_{30}$  and  $Y_{21}$  values were derived by comparison of the experimental and calculated line intensities and the node positions in the continua.

These steps were repeated iteratively until the computed and experimental data were in agreement. The convergence criterion was that the change in the spectroscopic constants from one step to the next was less than the initial errors in those constants (derived from the term values only). Taking into account that the line intensities are much more strongly influenced by subtle details of the potentials and other factors which we have excluded above in our considerations ( $M(R)$ , non-adiabatic intermixing), their weights in the fitting procedure were taken to be less than that of the continua node positions. The term value of the rovibrational level ( $v = v_x + 1$ ,  $N =$

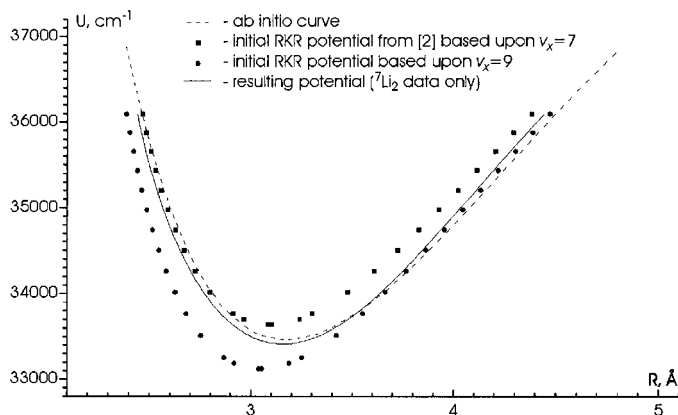


FIG. 4. Potential energy curves for the 3<sup>3</sup>Π<sub>g</sub> state of the Li<sub>2</sub> molecule. The *ab initio* curve (dashed line) is from (2). The potential produced from the data analysis of the present work (solid line) is based on the <sup>7</sup>Li<sub>2</sub> data only.

4), which is evidently perturbed, was excluded from the analysis.

We were unable to find a satisfactory solution from this fitting procedure using either the  $v_x = 7$  or the  $v_x = 9$  vibrational numbering. The case  $v_x = 8$  was much more successful. The resulting spectroscopic constants are reported in Table 1, and the corresponding RKR potential energy curve, obtained from this global fit of the <sup>7</sup>Li<sub>2</sub> data, is shown in Fig. 4, in comparison to other variants. The resulting potential curve does, in fact, lie close to the one obtained from the smaller set of spectroscopic constants with the assumption  $v_x = 7$  at short internuclear distances, and close to the one obtained using the assumption  $v_x = 9$  at large separations, in agreement with the discussion above.

As an independent check of the results, we have computed the excitation probabilities from the intermediate window level <sup>7</sup>Li<sub>2</sub>  $b^3\Pi_u$  ( $v = 19$ ,  $N = 10$ ) into levels <sup>7</sup>Li<sub>2</sub> 3<sup>3</sup>Π<sub>g</sub> ( $v$ ,  $N =$

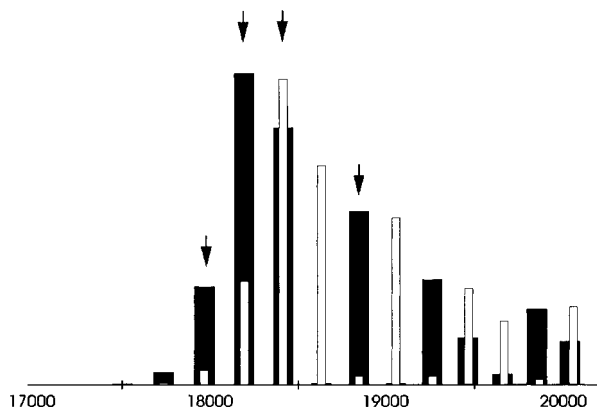


FIG. 5. Relative excitation probabilities for the <sup>7</sup>Li<sub>2</sub> 3<sup>3</sup>Π<sub>g</sub> ( $v$ ,  $N = 11$ ) ←  $b^3\Pi_u$  ( $v = 19$ ,  $N = 10$ ) transition, simulated with the initial potential from (2) (white bars) and with the potential of the present work based on the <sup>7</sup>Li<sub>2</sub> data (black bars). Arrows indicate transitions that were actually observed in the experiment.

TABLE 2  
Experimental <sup>6</sup>Li<sub>2</sub> Rovibrational Term Values (in cm<sup>-1</sup>) and Term Values Calculated from the 3<sup>3</sup>Π<sub>g</sub> Potential Obtained in the Present Work

$v$	$N$	term values (experiment)	term values calculated from spectroscopic constants obtained in this work ( <sup>7</sup> Li <sub>2</sub> data, $v_x = 8$ )
4	18	34776.883	34775.243
5	20	35067.149	35067.993
6	18	35274.693	35274.880
6	20	35315.043	35315.272

11), corresponding to the experimental conditions of (2), for two cases: (i) using the 3<sup>3</sup>Π<sub>g</sub> state potential curve from (2), (ii) using the 3<sup>3</sup>Π<sub>g</sub> state potential curve obtained in the present work from the <sup>7</sup>Li<sub>2</sub> data as described above. These results are shown in Fig. 5. In Ref. (2), only the vibrational levels  $v_x - 1$ ,  $v_x$ ,  $v_x + 1$ , and  $v_x + 3$  could be observed; excitation of the

TABLE 3  
Final Li<sub>2</sub> 3<sup>3</sup>Π<sub>g</sub> Potential Curve  $U(R)$  (in cm<sup>-1</sup>) and RKR Turning Points (in Å) Obtained in the Present Work Using all Available <sup>7</sup>Li<sub>2</sub> and <sup>6</sup>Li<sub>2</sub> Data

$v$	$R_{min}$	$R_{max}$	$U(R)$
-0.5	3.11805	3.13620	33406.3843
-0.25	2.99445	3.27265	33468.7872
0	2.94329	3.33667	33531.0525
1	2.82395	3.50747	33778.6812
2	2.74848	3.63448	34023.8806
3	2.69081	3.74382	34266.4677
4	2.64336	3.84311	34506.2593
5	2.60266	3.93588	34743.0725
6	2.56676	4.02412	34976.7241
7	2.53445	4.10910	35207.0312
8	2.50490	4.19172	35433.8107
9	2.47750	4.27264	35656.8795
10	2.45182	4.35237	35876.0546
11	2.42749	4.43134	36091.1530

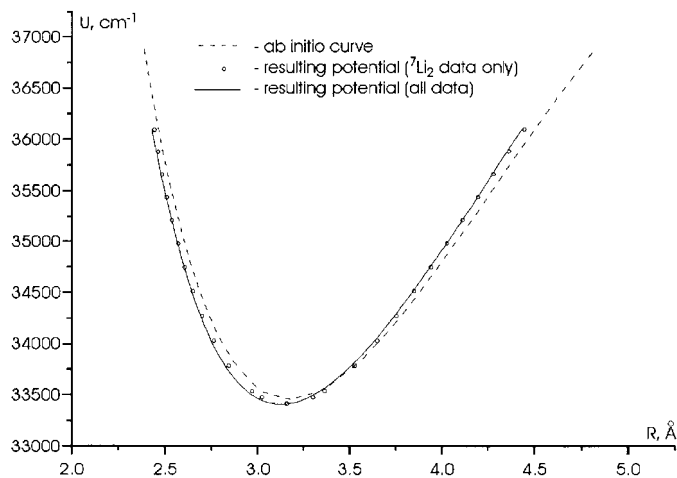


**FIG. 6.** Final  $\text{Li}_2$   $3^3\Pi_g$  RKR potential determined in this work using all  ${}^7\text{Li}_2$  and  ${}^6\text{Li}_2$  data (solid line), the  ${}^7\text{Li}_2$  data only (points), and *ab initio* curve (dashed line) from (2).

level  $v_x + 2$  from  $b^3\Pi_u$  ( $v = 19$ ,  $N = 10$ ) is apparently too weak for observation. This result is consistent with the simulated excitation probabilities based on the  $3^3\Pi_g$  state potential obtained from the  ${}^7\text{Li}_2$  data in the present work, but inconsistent with the simulation based on the earlier potential reported in (2).

All the measured continua and discrete spectra intensities are reproduced fairly well with this new potential. We have decided not to present their graphical comparisons because they do not differ visually from the analogous figures below for the final potential determined from all the experimental data (including the  ${}^6\text{Li}_2$  term values obtained after the analysis presented above was performed).

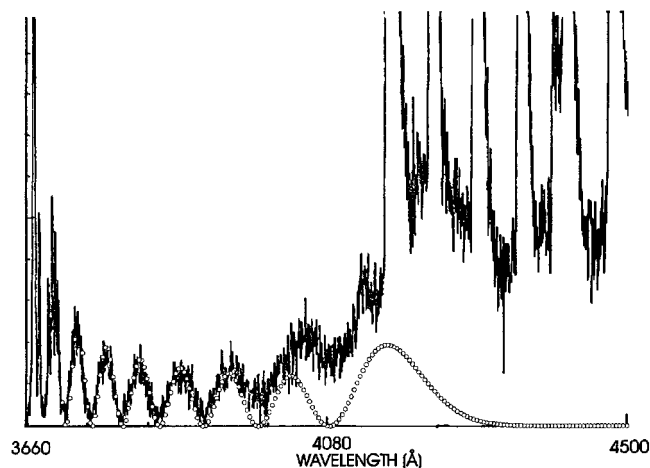


**FIG. 7.** Experimental  ${}^7\text{Li}_2$   $3^3\Pi_g$  ( $v = v_x$ ,  $N = 11$ )  $\rightarrow a^3\Sigma_u^+$  bound-free continuum and corresponding simulation based on the  $3^3\Pi_g$  state potential obtained in the present work from all  ${}^7\text{Li}_2$  and  ${}^6\text{Li}_2$  data using the assignment  $v_x = 8$ . The relative efficiency of the detection system as a function of wavelength (including polarization effects (17)) has been incorporated into the simulated spectrum for comparison to the raw experimental data.

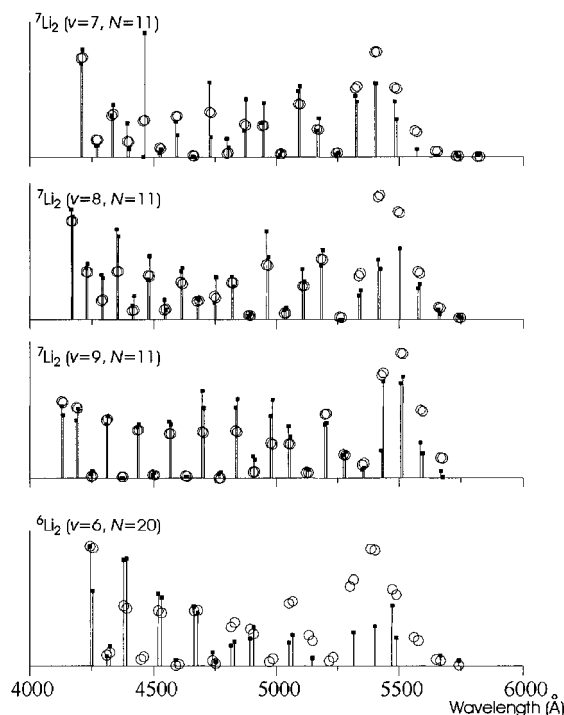


**FIG. 8.** Experimental  $\text{Li}_2$   $3^3\Pi_g$  ( $v, N$ )  $\rightarrow b^3\Pi_u$  line intensities (vertical lines) and relative intensities calculated using the  $3^3\Pi_g$  state potential obtained in the present work from all  ${}^7\text{Li}_2$  and  ${}^6\text{Li}_2$  data using the assignment  $v_x = 8$  (circles). In all cases, the observed transitions involve only the  $F_1$  ( $J = N + 1$ ) components of the upper and lower states. The experimental spectra have been corrected for the relative efficiency of the detection system (including polarization effects (17)) as a function of wavelength.

As a verification of the data analysis technique described above, including the revision of the vibrational numbering from that given in (2), we have carried out additional experimental measurements on the  ${}^6\text{Li}_2$  isotopomer. We have used the window level  $A^1\Sigma_u^+$  ( $v' = 9$ ,  $J' = 20$ )  $\sim b^3\Pi_u$  ( $v' = 15$ ,  $N' = 19$ ) (6) to measure four  ${}^6\text{Li}_2$  term values which are listed in Table 2. The isotope shift provides an absolute determination of the vibrational numbering and confirms the value  $v_x = 8$  obtained in the analysis described above.

When calculating the isotopically shifted term values, we have taken into account the fact that for rotational quantum numbers near  $N = 20$ , the spectroscopic constant  $Y_{02}$ , neglected above, gives a significant contribution  $\sim -1 \text{ cm}^{-1}$ . The value of the  $Y_{02}$  constant was estimated using the well-known relation (see, e.g., (14))

$$Y_{02} = -4Y_{01}^3/Y_{10}^2 \quad [1]$$

from the constants determined above. The predicted term value  $T_{v=4, N=18}$  in Table 2 differs from the experimental one strongly, so we can suggest that it is perturbed; this suggestion was independently confirmed by fitting a truncated set of only five constants from all  ${}^7\text{Li}_2$  and  ${}^6\text{Li}_2$  experimental term values.

**TABLE 4**  
**Li<sub>2</sub> 3<sup>3</sup>Π<sub>g</sub> Rovibrational Level Term Values (in cm<sup>-1</sup>) Calculated with Different Potential Functions and Compared with the Experimental Values**

	experiment	final potential (this work)				initial Dunham fit from [2]	theoretical [2]		
<i>N</i>	<i>E</i>	<i>v</i>	<i>E</i> from RKR potential	<i>E</i> from spectroscopic constants	difference of term values; observed - calculated (from final spectroscopic constants)	<i>v</i>	<i>E</i> from spectroscopic constants	<i>v</i>	<i>E</i> from smoothed potential
<sup>7</sup> Li <sub>2</sub> data									
9	35246.877	7	35246.774	35246.754	0.123	6	35246.714	7	35257.719
11	35265.592	7	35265.488	35265.477	0.115	6	35265.659	7	35275.930
4	35442.167	8	35442.203	35442.089	0.078	7	35442.186	8	35448.090
5	35446.520	8	35446.617	35446.506	0.014	7	35446.593	8	35452.382
6	35451.855	8	35451.913	35451.803	0.052	7	35451.882	8	35457.530
9	35472.994	8	35473.073	35472.973	0.021	7	35473.037	8	35478.104
11	35491.452	8	35491.559	35491.469	-0.007	7	35491.547	8	35496.081
4	35665.811	9	35665.171	35664.980	0.831	8	35665.501	9	35665.254
6	35675.031	9	35674.765	35674.577	0.454	8	35674.969	9	35674.569
9	35695.658	9	35695.671	35695.491	0.167	8	35695.628	9	35694.871
11	35713.803	9	35713.935	35713.764	0.039	8	35713.704	9	35712.610
9	36129.120	11	36129.034	36128.754	0.366	10	36129.615	11	36117.027
11	36146.790	11	36146.868	36146.588	0.202	10	36146.822	11	36134.274
<sup>6</sup> Li <sub>2</sub> data									
18	34776.883	4	34774.433	34774.828	2.055	3	34760.189	4	34797.174
20	35067.149	5	35067.261	35067.638	-0.489	4	35054.549	5	35082.826
18	35274.693	6	35274.635	35274.836	-0.143	5	35259.394	6	35324.174
20	35315.043	6	35314.949	35315.218	-0.175	5	35300.959	6	35284.889

Note. The experimental measurement error is ~0.01 cm<sup>-1</sup>.

The level (*v* = 4, *N* = 18) has been excluded from the following analysis.

In addition, we recorded resolved <sup>6</sup>Li<sub>2</sub> 3<sup>3</sup>Π<sub>g</sub> (*v* = 6, *N* = 20) → *b*<sup>3</sup>Π<sub>u</sub> bound-bound fluorescence line intensities.

The new <sup>6</sup>Li<sub>2</sub> data have been combined with the previous <sup>7</sup>Li<sub>2</sub> data in one last global fit to produce a best set of spectroscopic constants (listed in Table 1 as the “final spectroscopic constants”). The final RKR potential curve is listed in Table 3 and plotted in Fig. 6 along with the *ab initio* curve from (2) and the potential obtained from the <sup>7</sup>Li<sub>2</sub> data only. The fitting procedure was improved by two additional steps.

1. The constant *Y*<sub>02</sub> was incorporated by using Eq. [1] with the *Y*<sub>01</sub> and *Y*<sub>10</sub> values determined in the previous step of the procedure.

2. The electronic transition dipole moments function *M*(*R*) of the 3<sup>3</sup>Π<sub>g</sub> → *b*<sup>3</sup>Π<sub>u</sub> and 3<sup>3</sup>Π<sub>g</sub> → *a*<sup>3</sup>Σ<sub>u</sub><sup>+</sup> transitions were estimated in the linear approximation *M*(*R*) = 1 + *m*<sub>1</sub>*R* and used in calculations of the bound-bound line and bound-free continuum intensities. The *m*<sub>1</sub> coefficients were obtained by the fits of the overall line and continuum intensities and corrected several times during computations. The final values are *m*<sub>1</sub> ≈ 0.2 (Å)<sup>-1</sup> for the 3<sup>3</sup>Π<sub>g</sub> → *b*<sup>3</sup>Π<sub>u</sub> transition and *m*<sub>1</sub> ≈ -0.167 (Å)<sup>-1</sup> for the 3<sup>3</sup>Π<sub>g</sub> → *a*<sup>3</sup>Σ<sub>u</sub><sup>+</sup> transition.

The  ${}^7\text{Li}_2\ 3^3\Pi_g\ (v_x, N = 11) \rightarrow a^3\Sigma_u^+$  continuum, simulated using this resulting potential and transition dipole moment, is compared to the experimental one in Fig. 7. The comparison of the simulated and experimental line intensities of the  $3^3\Pi_g\ (v, N) \rightarrow b^3\Pi_u$  spectra for both  ${}^7\text{Li}_2$  and  ${}^6\text{Li}_2$  isotopomers is shown in Fig. 8. The profile of the continuum is reproduced very well. The accuracy of the line intensity simulations, compared to the initial case  $v_x = 7$ , is of the same quality for the first six lines and is much better for those at the long wavelength end of the band. The remaining discrepancies in the line intensities can be explained by the factors mentioned above which were neglected in this analysis. An analogous result was also obtained for the  ${}^7\text{Li}_2\ 3^3\Pi_g\ (v_x + 1, N = 11) \rightarrow a^3\Sigma_u^+$  continuum.

In summary, we conclude that the  ${}^7\text{Li}_2\ 3^3\Pi_g$  vibrational numbering ( $v_x = 7$ ) previously reported in (2) should be corrected to  $v_x = 8$ , and that the final spectroscopic constants reported in Table 1 of the present work give the best representation of all available  ${}^7\text{Li}_2$  and  ${}^6\text{Li}_2$  experimental data. We note that the inclusion of bound-free continua node positions and bound-bound spectra line intensities in a global fit with the measured term values, as described here, can lead to significant improvements in spectroscopic constants and RKR potentials obtained from limited data sets.

### 3. DISCUSSION

As seen in Figs. 4 and 6, the  $\text{Li}_2\ 3^3\Pi_g$  potential curve obtained in the current work as described above agrees best, among the alternatives presented, with the theoretical *ab initio* potential function of (2). This agreement is also reflected in the spectroscopic constants of Table 1 and in the comparison of the experimental and calculated ro-vibrational term values of Table 4 (where one should take note of the vibrational assignments).

Notice that the rovibrational term values calculated from the final RKR potential (Table 4) demonstrate small, but regular, discrepancies (of different sign for the two isotopomers) from the observed values, even though the input spectroscopic constants of the RKR procedure reproduce the experimental term values very well. The origin of this discrepancy is obviously the first-order WKB approximation used in the RKR procedure. Figure 9 presents a comparison of the theoretical potential of the  $3^3\Pi_g$  state and its RKR reconstruction, demonstrating this error. [The latter was obtained by first fitting a set of spectroscopic constants (Table 1) to the eigenvalues of the exact theoretical potential, and then using these constants to obtain the RKR curve.] Our test computation has shown that this error can result in an  $\sim 0.2\%$  mean-squared error in the  $3^3\Pi_g \rightarrow b^3\Pi_u$  relative line intensities (over the range observed) and in an  $\sim 0.05\%$  mean-squared error in the  $3^3\Pi_g \rightarrow a^3\Sigma_u^+$  continuum node positions (over the observed range of the continuum). Such an error is sufficiently small that there is no need to revise the results of the present paper. However,

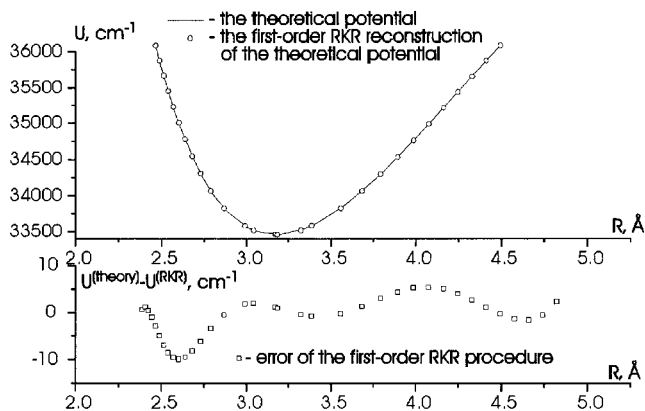


FIG. 9. Comparison of the theoretical  $\text{Li}_2\ 3^3\Pi_g$  state potential curve and its reconstruction by the lowest order RKR procedure.

more precise results for the potential function can be obtained by using the bound state IPA (Inverse Perturbation Approach) procedure (15). The third-order RKR procedure of (16) requires knowledge of  $3^3\Pi_g$  ro-vibrational term values of the two isotopomers in approximately the same region of energies and, hence, cannot be used here.

### ACKNOWLEDGMENTS

The authors thank Hongmin Chen for valuable discussions. This work was supported by the Russian Foundation for Basic Research (Grants 96-03-00035c and 96-03-32797a), the National Natural Science Foundation of China (Grant 29573110), and the U.S. National Science Foundation (Grant CHE-9320110).

### REFERENCES

1. L. Li and R. W. Field, *J. Phys. Chem.* **87**, 3020 (1983).
2. A. Yiannopoulou, K. Urbanski, S. Antonova, A. M. Lyyra, L. Li, T. An, T. J. Whang, B. Ji, X. T. Wang, W. C. Stwalley, T. Leininger, and G.-H. Jeung, *J. Chem. Phys.* **103**, 5898 (1995).
3. V. S. Ivanov and V. B. Sovkov, *Opt. Spectrosc.* **74**, 52 (1993).
4. V. S. Ivanov and V. B. Sovkov, *Chem. Phys.* **213**, 295 (1996).
5. V. S. Ivanov and V. B. Sovkov, *Proc. SPIE* **3090**, 150 (1997); *Opt. Spectrosc.* **83**, 836 (1997).
6. X. Xie and R. W. Field, *Chem. Phys.* **99**, 337 (1985).
7. M. S. Aleksandrov, V. A. Elokhin, and V. S. Ivanov, Depository by All-Union Institute of Scientific and Technical Information N 4213-81, pp. 71–82, Leningrad, 1981 [in Russian]; J. M. Cooley, *Math Comp.* **15**, 363 (1961); J. M. Blatt, *J. Comp. Phys.* **1**, 382, (1967); R. J. Le Roy, R. G. Macdonald, and G. Burns, *J. Chem. Phys.* **65**, 6699 (1976).
8. I. Schmidt-Mink, W. Müller, and W. Meyer, *Chem. Phys.* **92**, 263 (1985).
9. A. Yiannopoulou, K. Urbanski, A. M. Lyyra, L. Li, B. Ji, J. T. Bahns, and W. C. Stwalley, *J. Chem. Phys.* **102**, 3024 (1995).
10. W. Preuss and G. Baumgartner, *Z. Phys. A* **320**, 125 (1985); X. Xie and R. W. Field, *J. Mol. Spectrosc.* **117**, 228 (1986).
11. M. S. Child, H. Esssen, and R. J. Le Roy, *J. Chem. Phys.* **78**, 6732 (1983).

12. R. J. Le Roy and R. B. Bernstein, *J. Chem. Phys.* **52**, 3869 (1970); W. C. Stwalley, *Chem. Phys. Lett.* **6**, 241 (1970).
13. A.-R. Hashemi-Attar, C. L. Beckel, W. N. Keepin, and S. A. Sonnleitner, *J. Chem. Phys.* **70**, 3881 (1979); C. L. Beckel and R. B. Kwong, *J. Chem. Phys.* **73**, 4698 (1980); C. L. Beckel, R. B. Kwong, A.-R. Hashemi-Attar, and R. J. Le Roy, *J. Chem. Phys.* **81**, 66 (1984).
14. J. K. G. Watson, *J. Mol. Spectrosc.* **80**, 411 (1980).
15. M. M. Kosman and J. Hinze, *J. Mol. Spectrosc.* **56**, 93 (1973); H. Helm, in "SASP'84: Symp. Atom. and Surface Phys., Maria Alm, Salzburg, 29 Jan.–4 Febr., 1984," Contrib., Innsbruck, p. 16; C. R. Vidal and H. Scheingraber, *J. Mol. Spectrosc.* **65**, 46 (1977); G. Gouedard and J. Vigue, *Chem. Phys. Lett.* **96**, 293 (1983); I. P. Hamilton, J. C. Light, and K. B. Whaley, *J. Chem. Phys.* **85**, 5151 (1986); C. R. Vidal and W. C. Stwalley, *J. Chem. Phys.* **77**, 883 (1982); J. M. Hutson, *J. Phys. B.* **14**, 851 (1981).
16. C. Schwartz and R. J. LeRoy, *J. Chem. Phys.* **81**, 3996 (1984).
17. H. Chen, L. Li, G. Lazarov, A. M. Lyra, J. Huenekens, and R. W. Field, submitted for publication.